Ionics (2018) 24:1595–1602
https://doi.org/10.1007/s11581-017-2329-x

ORIGINAL PAPER

Dandelion-like mesoporous Co_3O_4 as anode materials for lithium ion batteries

Rihui Zhou[1] · Yaqin Chen[1] · Yuanyuan Fu[1] · Yanfei Li[1] · Shouhui Chen[1] · Yonghai Song[1] · Li Wang[1]

Received: 13 October 2017 / Accepted: 27 October 2017 / Published online: 3 November 2017

Abstract A dandelion-like mesoporous Co_3O_4 was fabricated and employed as anode materials of lithium ion batteries (LIBs). The architecture and electrochemical performance of dandelion-like mesoporous Co_3O_4 were investigated through structure characterization and galvanostatic charge/discharge test. The as-prepared dandelion-like mesoporous Co_3O_4 consisted of well-distributed nanoneedles (about 40 nm in width and about 5 μm in length) with rich micropores. Electrochemical experiments illustrated that the as-prepared dandelion-like mesoporous Co_3O_4 as anode materials of LIBs exhibited high reversible specific capacity of 1430.0 mA h g^{-1} and 1013.4 mA h g^{-1} at the current density of 0.2 A g^{-1} for the first and 100th cycle, respectively. The outstanding lithium storage properties of the as-prepared dandelion-like mesoporous Co_3O_4 might be attributed to its dandelion-like mesoporous nanostructure together with an open space between adjacent nanoneedle networks promoting the intercalation/deintercalation of lithium ions and the charge transfer on the electrode. The enhanced capacity as well as its high-rate capability made the as-prepared dandelion-like mesoporous Co_3O_4 to be a good candidate as a high-performance anode material for LIBs.

Keywords Dandelion-like mesoporous Co_3O_4 · Anode materials · Lithium ion batteries

Introduction

Lithium ion batteries (LIBs) have attracted extensive interest owing to its high energy density, long cycle life, slight memory effect, small volume, and environmental friendliness [1–6]. In the past few years, lots of attempts were carried out to explore various outstanding lithium ion storage nanomaterials for meeting the need of portable electronic devices, such as smartphone, laptop, smartwatch, etc. So far, several anode materials have been exploited, such as transition metal oxides (TMOs) nanomaterials [7–11], carbon-based nanomaterials [12–16], and various alloy nanomaterials [17–21]. Among various TMOs, Co_3O_4 was a fascinating LIBs' anode material owing to its high theoretical specific capacity (890 mA h g^{-1}), low cost, abundance, and environmental friendliness. Nevertheless, the extensive application of Co_3O_4-based anodes was limited due to its huge volume expansion effect in the process of charge/discharge.

To solve the problem, an effective approach was to fabricate mesoporous Co_3O_4-based nanomaterials as potential electrode materials. Some unique mesoporous Co_3O_4-based nanomaterials have been developed, such as flower ball-like Co_3O_4 [14], dumbbell-like Co_3O_4 [22], flower-like Co_3O_4 [23], Co_3O_4 cubes [24], snowflake-like sheets [25], yolk-shell Co_3O_4 microspheres [26], and bowknot-like Co_3O_4 [27]. The mesoporous Co_3O_4-based nanomaterials usually exhibited good performance due to their large specific surface area, a large number of holes effectively inhibiting the structural collapse and potential hazards caused by volume expansion in the process of charge/discharge, and rapid mass transfer between the electrolyte and the active material. For

Electronic supplementary material The online version of this article (https://doi.org/10.1007/s11581-017-2329-x) contains supplementary material, which is available to authorized users.

✉ Li Wang
lwanggroup@aliyun.com

[1] Key Laboratory of Functional Small Organic Molecule, Ministry of Education, Key Laboratory of Chemical Biology, Jiangxi Province, College of Chemistry and Chemical Engineering, Jiangxi Normal University, Nanchang 330022, China

example, cluster-like Co_3O_4 delivered a high reversible capacity of 1067 mA h g^{-1} at a current density of 0.1 A h g^{-1} after 100 cycles [28]. Mesoporous Co_3O_4 microdisks exhibited a stable specific discharge/charge capacity of 765 and 749 mA h g^{-1} after 30 cycles at a current density of 0.1 A h g^{-1} [29]. Hydrotalcite-like Co_3O_4 released the initial capacities of 756 mA h g^{-1} and remained 582 mA h g^{-1} at the 100th cycle under the current density of 0.8 A h g^{-1} [11]. The results clearly indicated that the structure was crucial to improve the performance of Co_3O_4-based anode materials. Accordingly, the designation and synthesis of mesoporous Co_3O_4-based nanomaterials owning special distribution of pore and particle sizes were still very necessary for further improvement of performance.

Herein, a new mesoporous dandelion-like Co_3O_4 nanomaterial was synthesized. The as-prepared dandelion-like mesoporous Co_3O_4 consisted of well-distributed nanoneedles which were about 50 nm in width and about 5 μm in length. The nanoneedles were composed of small Co_3O_4 nanoparticles, which formed many micropores. The opened porous feature enables full utilization of active materials and rich accessibility of the electrolyte. The ultra-small and Co_3O_4 nanocrystals produced a large number of active sites. Meanwhile, the interspaces among the Co_3O_4 nanoneedles and among small Co_3O_4 nanocrystals provide extra and sufficient space to further alleviate the volume expansion effect during lithiation and delithiation. As a result, the as-prepared Co_3O_4 mesoporous dandelion-like Co_3O_4 nanomaterial demonstrates superior electrochemical performance of LIBs when evaluated as anode materials.

Experimental

Materials

Cobalt nitrate hexahydrate ($Co(NO_3)_2 \cdot 6H_2O$, analytical grade), ammonium fluoride (NH_4F, analytical grade), and urea ($CO(NH_2)_2$, analytical grade) were obtained from Aladdin Industrial Corporation. Polyvinylidene fluoride (PVDF), carbon black, and ethanol were purchased from Guangdong Xilong Chemical Reagent Factory (Guangzhou, China). Metallic Li foil (0.6-mm thickness, 99.9%) was purchased from Zhongneng Tianjin and copper foil (10-μm thickness) came from Jiayuan Guangzhou Company (Guangzhou, China). In this paper, Millipore-Q System (18.2 MΩ cm) was used to prepare ultra-pure water. In addition, all chemical reagents used in this work were without further purification.

Preparation of the mesoporous dandelion-like Co_3O_4

The mesoporous dandelion-like Co_3O_4 nanomaterial was synthesized via hydrothermal method followed by calcination at 400 °C in air. Firstly, 1-mmol Co $(NO_3)_2 \cdot 6H_2O$, 2-mmol NH_4F, and 5-mmol urea were added into 70-mL ultra-pure water in sequence with magnetic stirring for 30 min. Then, the mixture was transferred to a 100-mL Teflon-lined stainless autoclave. The autoclave was sealed and maintained at 110 °C in an electric oven for 5 h. Once the reaction was completed, the autoclave was allowed to cool down to room temperature. The obtained precursor was then washed for several times using distilled water followed by ethanol and further dried at 80 °C in vacuum for 8 h. Finally, the dandelion-like Co_3O_4 nanomaterials were obtained by placing the precursor to a tube furnace and heated up to 400 °C at the ramping rate of 10 °C /min and held for 2 h under air atmosphere.

Characterization

Scanning electron microscopy (SEM) images were obtained with a Hitachi S3400N at an accelerating voltage of 20 kV equipped with an energy dispersive spectrometer (EDS). X-ray powder diffraction (XRD) data were taken by a Bruker D8 Advanced X-ray powder diffractometer using Cu Kα radiation. Thermogravimetric analysis was performed on Perkin-Elmer Pyris Diamond thermogravimetric/differential thermal analysis (TG/DTA) instrument with a heating rate of 10 °C min^{-1}. Fourier transform infrared spectroscopy (FT-IR) was conducted on a Nicolet 6700 FTIRATR spectrometer. Raman spectra were recorded on a LabRAM HR (Horiba Jobin Yvon) with a 633-nm laser. N_2 adsorption/desorption isotherms were measured at −196 °C, using a BELSORP-mini II instrument. Before the measurement, the samples were degassed for 3 h under vacuum at 150 °C. The surface area, pore volume, and pore size distribution of the samples were estimated based on N_2 adsorption/desorption isotherm. Transmission electron microscopy (TEM) images were obtained through the instrument of JEOL JEM-2100 microscopes which were conducted at an acceleration voltage of 200 kV.

Electrochemical measurements

The working electrode was derived from homogeneous slurry including active material, acetylene black and PVDF with weight ratio about 8:1:1. The slurry was dispersed evenly on copper foil which plays the role as a current collector. Then, it was dried under 60 °C in a vacuum oven for all night. The active material loading on the copper foil was approximately 0.95 mg cm^{-2}. The separator was a Celgard 2300 microporous polypropylene film. The full cell was assembled in an argon-filled glove box. The electrolyte was composed of 1.0-M $LiPF_6$, ethylene carbonate, diethyl carbonate, and dimethyl carbonate. Finally, galvanostatic charge/discharge was cycled at potential range from 3.0 to 0.01 V versus Li/Li^+. Cyclic voltammograms (CVs) and electrochemical impedance

spectroscopy (EIS) were determined by a CHI 760E electrochemical workstation which comes from CH Instruments in Shanghai. Li metal acted as the counter and reference electrode and the target materials acted as the working electrode. The electrochemical discharge/charge performance and rate performance testing were carried out on a Neware BTS test system (Shenzhen, China) at voltage range from 3.0 to 0.01 V versus Li/Li^+.

Results and discussion

Figure S1 (Supporting Information) showed the TG/DTA curves of the precursor powder, with a heating rate of 10 °C min^{-1} in air. Firstly, the thermal decomposition of the residual molecules in the pores caused the weight loss of 4.3 wt% at about 200 °C. With the increase of temperature, there was a marked weight loss of 21.6 wt% due to the precursor being transformed into Co_3O_4 between 220 and 380 °C. And there was a corresponding endothermic peak at the DTA curve. No obvious weight losses for the precursor were found after 400 °C, suggesting the complete conversion from the precursor to Co_3O_4. In order to obtain the final Co_3O_4 material with relatively high purity and crystalline, 400 °C was chosen as the suitable calcined temperature.

The element composition of Co_3O_4 was determined by EDS analysis as shown in Fig. 1a. Only peaks related to Co and O elements were found and no other peaks appeared. The atomic ratio of Co to O in the sample was 44.31:55.69, confirming the formation of Co_3O_4 with high purity. Meanwhile, the characterization of XRD, FT-IR, and Raman spectroscopy was also carried out. For the XRD pattern (Fig. 1b), the diffraction peaks at 19.0°, 31.3°, 36.8°, 38.6°, 44.8°, 55.7°, 59.4°, and 65.3° could be denoted as the 111, 220, 311, 222, 400, 422, 511, and 440 lattice planes of spinel Co_3O_4 oxide (JCPDS#42-1467) [30, 31, 34, 36], respectively. The FT-IR spectra of Co_3O_4 displayed two sharp bands at 571.16 and 664.68 cm^{-1} originating from the stretching vibration of the metal-oxygen bonds (ν(Co–O)) in the spinel lattice as shown in Fig. 1c. The bands centered at 1633.12 and 3475.27 cm^{-1} were assigned to the hydroxyl group (−OH) stretching and bending modes of water [32]. Raman spectrum of as-prepared Co_3O_4 was obtained to complement the FT-IR characterization. As shown in Fig. 1d, the typical Raman peaks exhibited several peaks at 188, 462, 506, 608, and 663 cm^{-1} which were characteristics of cubic spinel Co_3O_4 [14, 31, 33].

The morphology of the as-fabricated precursor was characterized by SEM (Fig. 2a, b). It can be observed that the precursor looked like dandelion and consisted of numerous irregular nanoneedles with length ranging from 2 to 10 μm and diameter ranging from 30 to 50 nm. The morphology of the as-prepared Co_3O_4 was consistent with that of the precursor as shown in Fig. 2c, d. The dandelion-like structure of the as-prepared Co_3O_4 showed some open space between adjacent nanoneedles, which would contribute to the diffusion of electrolyte, alleviating volume expansion effect and enhancing the rate performance.

Figure 3a, b showed the TEM images of the as-prepared dandelion-like Co_3O_4, revealing the details of morphology directly. The TEM images confirmed that the nanoneedles were consisted of lots of small spherical nanoparticles with 20 nm in diameter. Figure 3a, b also revealed many mesopores among the small Co_3O_4 nanoparticles. Figure 3c was the HRTEM image of the Co_3O_4 which showed distinct lattice fringes with interplanar spacings of 0.466, 0.286, 0.243, 0.233, and 0.202 nm, corresponding to the 111, 220, 311, 222, and 400 crystal planes of Co_3O_4, respectively [1, 24, 35, 36]. The HRTEM image matched well with the standard PDF pattern (JCPDS#42-1467). Meanwhile, the resulted Co_3O_4 had the properties of a polycrystalline phase as shown by selected area electron diffraction (SAED) in Fig. 3d. The result confirmed that the porous dandelion-like Co_3O_4 was a polycrystal consisting of single-crystal nanoparticles.

To further analyze the porous structure of the dandelion-like Co_3O_4, the pore size distribution and specific surface area were measured using BJH and BET methods, respectively. As shown in Fig. 4, the dandelion-like Co_3O_4 displayed a narrow pore size distribution, which was mainly concentrated in the range of 1.00 to 30.00 nm with an average pore diameter of 20.29 nm. Meanwhile, the specific surface area was calculated to be about 27.6 $m^2\ g^{-1}$, according to the information obtained by nitrogen adsorption/desorption isotherm curve which was attributed to the type IV isotherm with a H4 hysteresis loop. The pore size distribution and specific surface area testified that the dandelion-like Co_3O_4 was a typical mesoporous structure which endowed the dandelion-like Co_3O_4 some superiority for lithium storage and diffusion, as well as enough space to accommodate large volume expansion during cycling.

The cycling and rate performances of the dandelion-like Co_3O_4 material were investigated as shown in Fig. 5. The 1st, 2nd, and 100th discharge and charge profiles of the mesoporous dandelion-like Co_3O_4 anode in the voltage range of 0.01–3.00 V (vs. Li^+/Li) at 0.2 A g^{-1} were carried out in Fig. 5a. There were two typical discharge plateaus at about 1.3 V (short plateau) and 1.1 V (long plateau) because of the decomposition of Co_3O_4 into Co^0 and the formation of a solid electrolyte interface (SEI) film, respectively [27]. As could be observed, the discharge capacities of 1st of 1427.9 mA h g^{-1}, 2nd of 1025.5 mA h g^{-1}, and 100th of 1013.4 mA h g^{-1} were all higher than the theoretical capacity of Co_3O_4 (890 mA h g^{-1}).

The electrochemical discharge/charge cycling testing of dandelion-like Co_3O_4 at the current density of 0.2 A g^{-1} for 100 cycles were exhibited in Fig. 5b. Results showed that the initial discharge/charge capacities of dandelion-like Co_3O_4

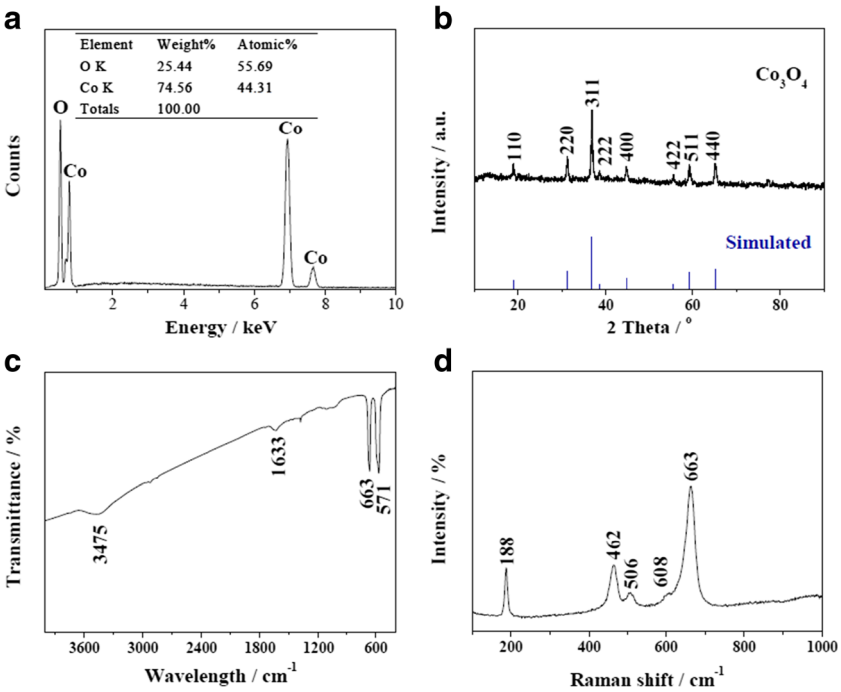

Fig. 1 **a** EDS curve, **b** XRD pattern, **c** FTIR spectra, and **d** Raman spectra of mesoporous dandelion-like Co_3O_4

were 1430.0 and 983.7 mA h g^{-1} with an initial coulombic efficiency of 71% and the following capacities tended towards increase until the 20th cycle leading to a stable capacity of 1032 mAh g^{-1}. Significantly, beyond the 1st cycle which showed a relatively low coulombic efficiency, the coulombic efficiencies for the subsequent cycles were generally maintained above 98%. After 100 cycles, a high charge specific capacity of 1013.4 mA h g^{-1} at 0.2 A g^{-1} with great capacity retention could also be observed. The extra capacity might result from the dandelion-like structure of the Co_3O_4 with open space between adjacent mesoporous nanoneedles and among small Co_3O_4 nanoparticles.

The rate performance of mesoporous dandelion-like Co_3O_4 was measured at various current densities from 0.2 to 5 A g^{-1} as shown in Fig. 5c. The capacity of mesoporous dandelion-like Co_3O_4 suffered a reduction with the increase of the current density. The mesoporous dandelion-like Co_3O_4 released the average specific capacity of 310 mA h g^{-1} at the high current density of 5 A g^{-1}, and it recovered to the capacity of 984.3 mA h g^{-1} when the current density returned to

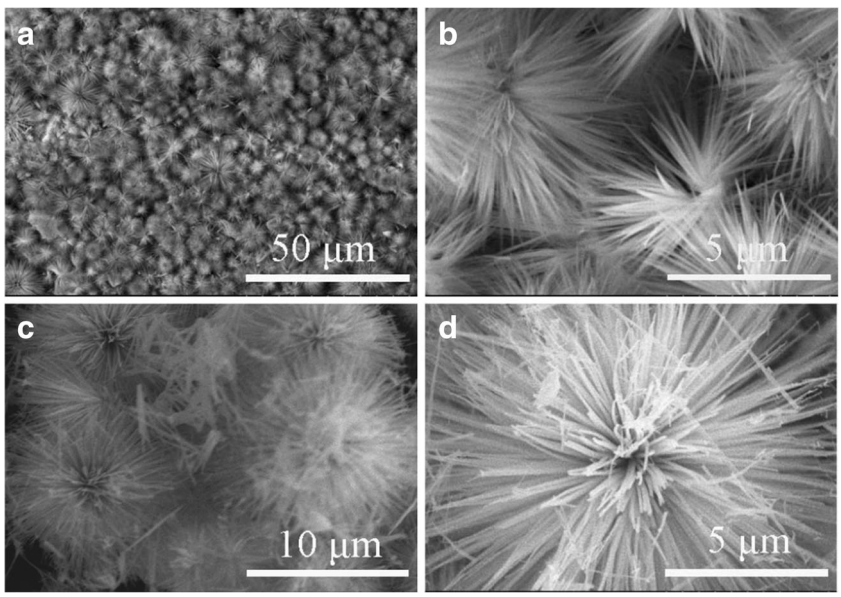

Fig. 2 **a**, **b** SEM images of the precursor. **c**, **d** SEM images of mesoporous dandelion-like Co_3O_4 at different magnifications

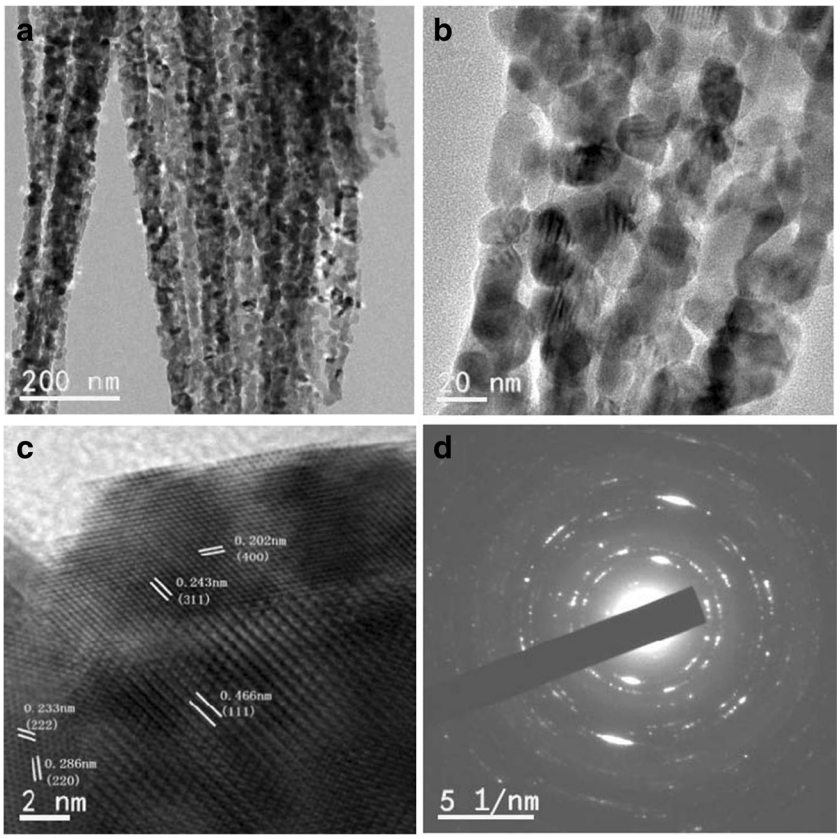

Fig. 3 **a**, **b** TEM images of the mesoporous dandelion-like Co_3O_4. **c**, **d** HRTEM image and SAED patterns of mesoporous dandelion-like Co_3O_4

0.2 A g^{-1}, implying that the capacity of the mesoporous dandelion-like Co_3O_4 had good recoverability. It was noteworthy that the charge capacity was still higher than the theoretical capacity.

Figure 5d exhibited the typical CV curves of mesoporous dandelion-like Co_3O_4 at the scan rate of 0.1 mV s^{-1} between the potential windows from 0.01 to 3.0 V. In the first cycle, the cathodic peak at 0.83 V was attributed to the electrochemical reduction of Co_3O_4 to metallic Co accompanying with the formation of amorphous Li_2O, the decomposition of electrolyte, and the formation of solid electrolyte interface (SEI) film [34, 35]. In the subsequent anodic process, there was a significant peak around 2.08 V which might represent the formation of Co_3O_4 and the decomposition of amorphous Li_2O. In the second cycle, there were two reduction peaks at 0.95 and 1.11 V, possibly originated from the complex multi-step reaction behavior of $Co^{3+}/Co^{2+}/Co^0$ [35, 36]. At the same time, an oxidation peak could be observed at 2.13 V, arising from the reversible oxidation reaction of Co to Co_3O_4 [36]. Subsequently, the curves almost overlapped very well with other curves, which indicated that the mesoporous dandelion-like Co_3O_4 had good stability and superior reversibility as the anode material for LIBs, especially in cycling stability.

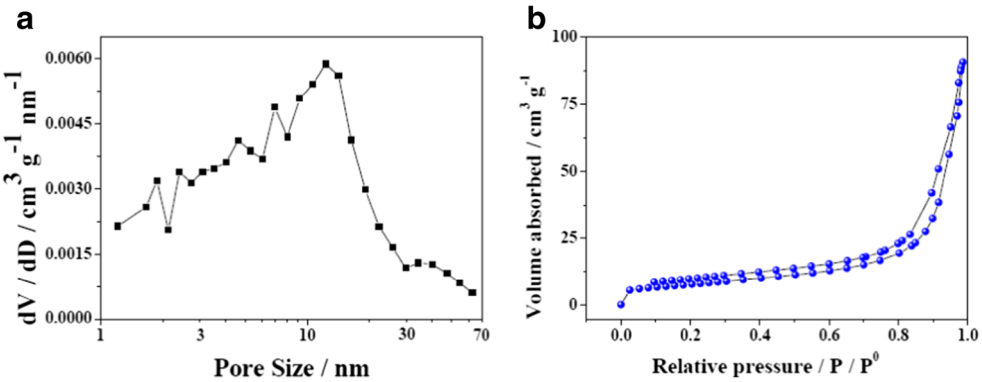

Fig. 4 **a** Pore size distribution and **b** nitrogen adsorption/desorption isotherm of mesoporous dandelion-like Co_3O_4

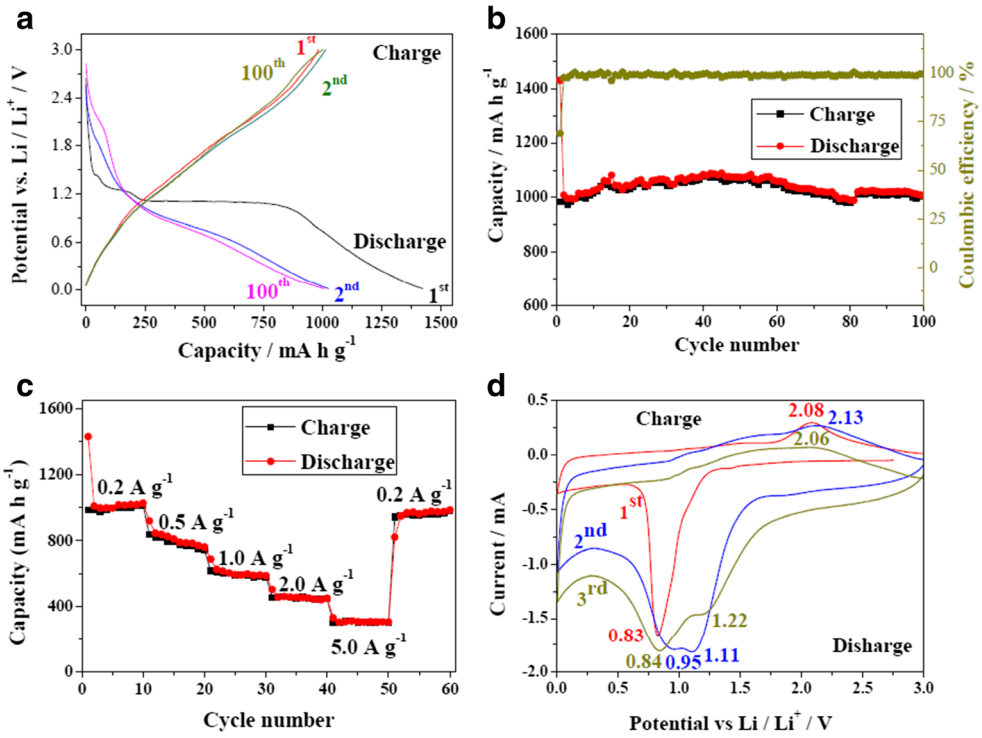

Fig. 5 **a** The 1st, 2nd, and 100th cycles charge and discharge profiles of the mesoporous dandelion-like Co_3O_4 electrode at 0.2 A g^{-1} between 0.01 to 3.0 V. **b** Cycling performance of mesoporous dandelion-like Co_3O_4 at 0.2 A g^{-1}. **c** Rate capacities of mesoporous dandelion-like Co_3O_4. **d** CV curves of mesoporous dandelion-like Co_3O_4 electrode for the first 3 cycles, with a 0.1 mV s^{-1} scan rate in the range of 0.01 to 3.0 V

To better understand the electrical conductivity and the charge transfer efficiency of the mesoporous dandelion-like Co_3O_4, EIS analysis was carried out before the first cycle and after the 100th cycles at a fully charged state. As shown in Fig. S2 (Supporting Information), the Nyquist impedance plots of Co_3O_4 were composed of a depressed semicircle in the high-frequency region and a sloping straight line in the low-frequency region. The former corresponded to the charge transfer resistance between electrode and electrolyte. The latter was assigned to the lithium diffusion resistance relating to the diffusion of lithium ions in the electrode [37]. Apparently, the battery demonstrated a larger diameter semicircle after 100 cycles, compared with the initial one, which was due to the charge transfer resistance increases.

In order to compare the performance of different Co-based anode materials, the electrochemical performance of several Co-based electrode materials and the as-prepared material was listed in Table 1. As shown in Table 1, the mesoporous dandelion-like Co_3O_4 electrode provided relatively higher capacity and enhanced cycling stability comparing with previously reported Co_3O_4-based anode materials.

In a word, Co_3O_4 with mesoporous dandelion-like structure as the anode material exhibited higher capacity and superior cycling stability. The possible reason for the improved electrochemical performances could be explained as follows. Firstly, the porous morphology with a high specific surface area was beneficial for shortening the diffusion lengths of lithium ions and providing more active sites. It makes the contact easier between the electrolyte and the active material.

Table 1 Comparison of the electrochemical performance of various Co_3O_4-based anode materials for LIBs

Active material	Current density mA g^{-1}	Initial coulombic efficiency %	N^{th} mA h g^{-1}	References
Co_3O_4 nanosheets	100	77.5	1067 (100)	[28]
Co_3O_4 microdisks	100	75.2	765 (30)	[29]
Co_3O_4 cuboids	100	51	886 (60)	[34]
rGO@Co_3O_4	100	70	974 (100)	[35]
Co_3O_4/C	200	74	928 (100)	[38]
Co_3O_4@TiO_2 CSNFs	180	69	632 (100)	[39]
Co_3O_4	100	74.4	683 (80)	[40]
Dandelion-like Co_3O_4	200	71	1013 (100)	This work

Secondly, the firm structure was very important to maintain a stable electrochemical performance. The dandelion-like Co_3O_4 material consisting of the special mesoporous structure could effectively decrease the agglomeration of nanoparticles and substantially alleviate the volume change during the whole charge/discharge process.

Conclusions

In summary, the mesoporous dandelion-like Co_3O_4 material was synthesized via a facile hydrothermal method followed by calcination at 400 °C in air. The dandelion-like Co_3O_4 material consisted of numerous nanoneedles which were composed of small nanoparticles, and strongly inherited the morphology of the precursor. The electrode material exhibited a higher first reversible charge capacity of 1430.0 mA h g^{-1}. Meanwhile, a super charge specific capacity of 1013.4 mA h g^{-1} was also observed after 100 cycles at 0.2 A g^{-1}. Moreover, the material also exhibited a satisfactory rate performance. The simplicity of the preparation method and the super electrochemical properties make the mesoporous dandelion-like Co_3O_4 material a candidate for the next generation of anode materials for LIBs.

Funding information This work was financially supported by the National Natural Science Foundation of China (21465014, 21665012, 21465015, and 21765009), Science and Technology Support Program of Jiangxi Province (20123BBE50104 and 20133BBE50008), Natural Science Foundation of Jiangxi Province (20143ACB21016), and the Ground Plan of Science and Technology Projects of Jiangxi Educational Committee (KJLD14023).

Compliance with ethical standards

Conflict of interest The authors declare that they have no conflicts of interest.

References

1. Kang B, Ceder G (2009) Battery materials for ultrafast charging and discharging. Nature 458:190–193
2. Li H, Wang Z, Chen L, Huang X (2009) Research on advanced materials for Li-ion batteries. Adv Mater 21:4593–4607
3. Chen S, Zhao Y, Sun B, Ao Z, Xie X, Wei Y, Wang G (2015) Microwave-assisted synthesis of mesoporous Co_3O_4 nanoflakes for applications in lithium ion batteries and oxygen evolution reactions. ACS Appl Mater Interfaces 7:3306–3313
4. Balogun MS, Yu M, Huang Y, Li C, Fang P, Liu Y, Lu X, Tong Y (2015) Binder-free Fe_2N nanoparticles on carbon textile with high power density as novel anode for high-performance flexible lithium ion batteries. Nano Energy 11:348–355
5. Liu S, Li L, Ahn HS, Manthiram A (2015) Delineating the roles of Co_3O_4 and N-doped carbon nanoweb (CNW) in bifunctional Co_3O_4/CNW catalysts for oxygen reduction and oxygen evolution reactions. J Mater Chem A 3:11615–11623
6. Wang D, He H, Han L, Lin R, Wang J, Wu Z, Liu H, Xin HL (2016) Three-dimensional hollow-structured binary oxide particles as an advanced anode material for high-rate and long cycle life lithium-ion batteries. Nano Energy 20:212–220
7. Wang C, Zhao Y, Su D, Ding C, Wang L, Yan D, Li J, Jin H (2017) Synthesis of NiO nano octahedron aggregates as high-performance anode materials for lithium ion batteries. Electrochim Acta 231: 272–278
8. Wang S, Li Q, Pu W, Wu Y, Yang M (2016) MoO_3-MnO_2 intergrown nanoparticle composite prepared by one-step hydrothermal synthesis as anode for lithium ion batteries. J Alloys Compd 663:148–155
9. Sun M, Sun M, Yang H, Song W, Nie Y, Sun S (2017) Porous Fe_2O_3 nanotubes as advanced anode for high performance lithium ion batteries. Ceram Int 43:363–367
10. Song Y, Chen Y, Fu Y, Li Y, Zhou R, Chen S, Wu J, Wang L (2017) Hollow multicomponent zeolitic imidazolate frameworks-derived $3NiO{\cdot}2Ni_{3/2}Co_{1/2}ZnO_4$ for high rate lithium-ion batteries. J Alloys Compd 703:148–155
11. Zhang X, Yang Z, Li C, Xie A, Shen Y (2017) A novel porous tubular Co_3O_4: self-assembly and excellent electrochemical performance as anode for lithium-ion batteries. Appl Surf Sci 403:294–301
12. Xu D, Luo G, Yu J, Chen W, Zhang C, Ouyang D, Fang Y, Yu X (2017) Quadrangular-CNT-Fe_3O_4-C composite based on quadrilateral carbon nanotubes as anode materials for high performance lithium-ion batteries. J Alloys Compd 702:499–508
13. Liu X, Li Z, Zhang S, Long H, Wei H, Zhang H, Li H, Zhao C (2017) Mo_2C@onion-like carbon/amorphous carbon nanocomposites as outstanding anode materials for ideal lithium-ion batteries. Ceram Int 43:14446–14452
14. Wang L, Fu Y, Chen Y, Li Y, Zhou R, Chen S, Song Y (2017) Ultralight flower ball-like Co_3O_4/melamine-derived carbon foam as anode materials for lithium-ion batteries. J Alloys Compd 724: 1117–1123
15. Song Y, Chen Y, Wu J, Fu Y, Zhou R, Chen S, Wang L (2017) Hollow metal organic frameworks-derived porous ZnO/C nanocages as anode materials for lithium-ion batteries. J Alloys Compd 694:1246–1253
16. Zhu S, Xu K, Sui S, Li J, Ma L, He C, Liu E, He F, Shi C, Miao L, Jiang J, Zhao N (2017) Synthesis of 2D/3D carbon hybrids by heterogeneous space-confined effect for electrochemical energy storage. J Mater Chem A 5:19175–19183
17. Xu Y, Liu Q, Zhu Y, Liu Y, Langrock A, Zachariah MR, Wang C (2013) Uniform nano-Sn/C composite anodes for lithium ion batteries. Nano Lett 13:470–474
18. Hong YJ, Son MY, Kang YC (2013) One-pot facile synthesis of double-shelled SnO_2 yolk-shell-structured powders by continuous process as anode materials for Li-ion batteries. Adv Mater 25:2279–2283
19. Zhu Y, Han X, Xu Y, Liu Y, Zheng S, Xu K, Hu L, Wang C (2013) Electrospun Sb/C fibers for a stable and fast sodium-ion battery anode. ACS Nano 7:6378–6386
20. Gao S, AM W, Jin XZ, Ye F, Dong XL, JY Y, Huang H (2017) Nanostructured Sn-M (M = Cu, Mg and Fe) intermetallic alloys and their electrochemical activity as anode electrodes in a Li-ion battery. J Alloys Compd 706:401–408
21. Gangaraju D, Sridhar V, Lee I, Park H (2017) Graphene-carbon nanotube-Mn_3O_4 mesoporous nano-alloys as high capacity anodes for lithium-ion batteries. J Alloys Compd 699:106–111
22. Wang X, Zhou B, Guo J, Zhang W, Guo X (2016) Selective crystal facets exposing of dumbbell-like Co_3O_4 towards high performances anode materials in lithium-ion batteries. Mater Res Bull 83:414–422
23. Liu W, Yang H, Zhao L, Liu S, Wang H, Chen S (2016) Mesoporous flower-like Co_3O_4/C nanosheet composites and their performance evaluation as anodes for lithium ion batteries. Electrochim Acta 207:293–300

24. Huang G, Xu S, Lu S, Li L, Sun H (2014) Micro-/nanostructured Co_3O_4 anode with enhanced rate capability for lithium-ion batteries. ACS Appl Mater Interfaces 6:7236–7243
25. Wang B, XY L, Tang Y (2015) Synthesis of snowflake-shaped Co_3O_4 with a high aspect ratio as a high capacity anode material for lithium ion batteries. J Mater Chem A 3:9689–9699
26. Son MY, Hong YJ, Kang YC (2013) Superior electrochemical properties of Co_3O_4 yolk-shell powders with a filled core and multishells prepared by a one-pot spray pyrolysis. Chem Commun 49:5678–5680
27. Du H, Yuan C, Huang K, Wang W, Zhang K, Geng B (2017) A novel gelatin-guided mesoporous bowknot-like Co_3O_4 anode material for high-performance lithium-ion batteries. J Mater Chem A 5:5342–5350
28. Wu S, Xia T, Wang J, Lu F, Xu C, Zhang X, Huo L, Zhao H (2017) Ultrathin mesoporous Co_3O_4 nanosheets-constructed hierarchical clusters as high rate capability and long life anode materials for lithium-ion batteries. Appl Surf Sci 406:46–55
29. Jin Y, Wang L, Shang Y, Gao J, Li J, He X (2014) Facile synthesis of monodisperse Co_3O_4 mesoporous microdisks as an anode material for lithium ion batteries. Electrochim Acta 151:109–117
30. Lu Z, Ding JJ, Lin X, Liu Y, Ye H, Yang G, Yin F, Yan B (2017) Low-temperature synthesis of two-dimensional nanostructured Co_3O_4 and improved electrochemical properties for lithium-ion batteries. Powder Technol 309:22–30
31. Pu Z, Zhou H, Zheng Y, Huang W, Li X (2017) Enhanced methane combustion over Co_3O_4 catalysts prepared by a facile precipitation method: effect of aging time. Appl Surf Sci 410:14–21
32. Ramamoorthy C, Rajendran V (2017) Effect of surfactants assisted Co_3O_4 nanoparticles and its structural, optical, magnetic and electrochemical properties. Optik 145:330–335
33. Porthault H, Baddour-Hadjen R, Cras FL, Bourbon C, Franger S (2012) Raman study of the spinel-to-layered phase transformation in sol-gel $LiCoO_2$ cathode powders as a function of the post-annealing temperature. Vib Spectrosc 62:152–158
34. Zheng F, Yin Z, Xia H, Zhang Y (2017) MOF-derived porous Co_3O_4 cuboids with excellent performance as anode materials for lithium-ion batteries. Mater Lett 197:188–191
35. Yin D, Huang G, Sun Q, Li Q, Wang X, Yuan D, Wang C, Wang L (2016) RGO/Co_3O_4 composites prepared using GO-MOFs as precursor for advanced lithium-ion batteries and supercapacitors electrodes. Electrochim Acta 215:410–419
36. Wu J, Zuo L, Song Y, Chen Y, Zhou R, Chen S, Wang L (2016) Preparation of biomass-derived hierarchically porous carbon/Co_3O_4 nanocomposites as anode materials for lithium-ion batteries. J Alloys Compd 656:745–752
37. Park GD, Cho JS, Kang YC (2015) Novel cobalt oxide-nanobubble-decorated reduced graphene oxide sphere with superior electrochemical properties prepared by nanoscale Kirkendall diffusion process. Nano Energy 17:17–26
38. Wang S, Zhu Y, Xu X, Sunarso J, Shao Z (2017) Adsorption-based synthesis of Co_3O_4/C composite anode for high performance lithium-ion batteries. Energy 125:569–575
39. Tong X, Zeng M, Li J, Liu Z (2017) Porous Co_3O_4@TiO_2 core-shell nanofibers as advanced anodes for lithium ion batteries. J Alloys Compd 723:129–138
40. Chen J, Mu X, Du M, Lou Y (2017) Porous rod-shaped Co_3O_4 derived from Co-MOF-74 as high-performance anode materials for lithium ion batteries. Inorg Chem Commun 84:241–245